Evaluation of solubility enhancement, antioxidant activity, and cytotoxicity studies of kynurenic acid loaded cyclodextrin nanosponge

EVALUATION OF SOLUBILITY ENHANCEMENT, ANTIOXIDANT ACTIVITY, AND CYTOTOXICITY STUDIES OF KYNURENIC ACID LOADED CYCLODEXTRIN NANOSPONGE.

Nilesh K. Dhakar[1], Fabrizio Caldera[1], Federica Bessone[2], Claudio Cecone[1], Alberto Rubin Pedrazzo[1], Roberta Cavalli[2], Chiara Dianzani[2], Francesco Trotta[1*]

[1]Department of Chemistry, University of Torino, via P. Giuria 7, 10125, Torino, Italy.

[2]Department of Drug Science and Technology, University of Torino, via P. Giuria 9, 10125, Torino, Italy.

***Corresponding author:**

Email: francesco.trotta@unito.it

Tel: 0116707550 Fax: 0116707855

Graphical Abstract

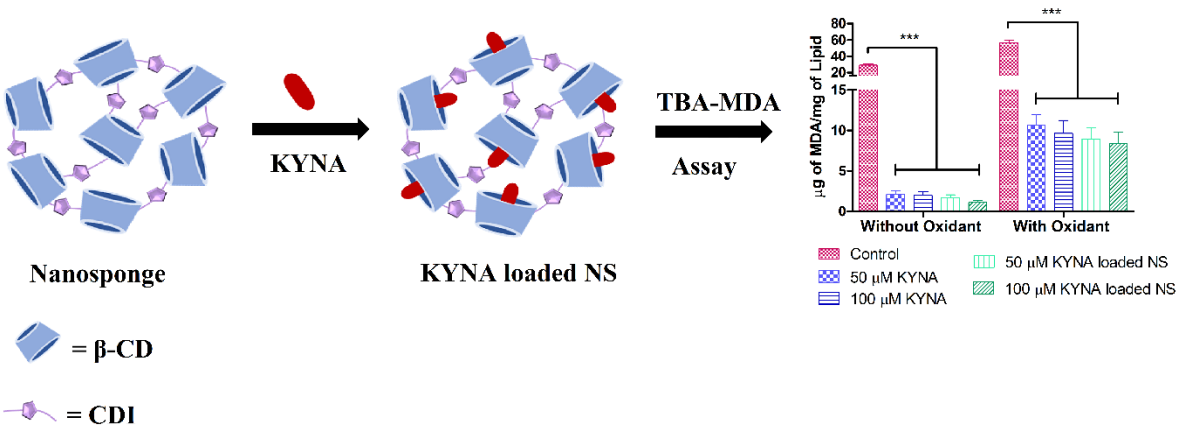

Highlights

- The aqueous solubility of KYNA was increased by encapsulation with β-CDNS2.
- The molar ratio of CDI to β-CD affected the solubilization efficiency of nanosponges.
- Higher antioxidant activity of KYNA loaded NS was achieved compared to plain KYNA.
- Cell viability study showed that NS was nontoxic to SHSY-5Y human neuroblastoma cell lines.
- The particle size and zeta potential of KYNA loaded NS and blank NS remained unchanged on storage.

Abstract

Kynurenic acid demonstrates antioxidant, neuroprotective and free radical scavenging properties. However, low aqueous solubility of kynurenic acid limits its therapeutic activity. In the present study, cyclodextrin nanosponges were used to improve the solubility and therapeutic activity of kynurenic acid. The formation of kynurenic acid loaded nanosponge was confirmed by different characterization techniques. The solubility of kynurenic acid was significantly increased with nanosponge (111.1 µg/ml) compared to free kynurenic acid (16.4 µg/ml) and β-cyclodextrin (28.6 µg/ml). High drug loading (19.06 %) and encapsulation efficiency (95.31 %) were achieved with NS. The particle size and zeta potential of kynurenic acid loaded nanosponge was around 255.8 nm and -23 mV respectively. Moreover, higher solubilization of kynurenic acid loaded nanosponge produced better antioxidant activity compared to free kynurenic acid. The kynurenic acid loaded nanosponge and blank nanosponge were found nontoxic in the cytotoxicity assay. Thus, these studies demonstrated that nanosponges can be used as a carrier for the delivery of kynurenic acid.

Keywords

Kynurenic acid, β-cyclodextrin, Nanosponges, Solubility Enhancement, Drug-Delivery, Antioxidant Activity

Abbreviations

KYNA: Kynurenic Acid, β-CD: Beta-cyclodextrin, CDI: N,N'-carbonyldiimidazole NS: Nanosponge, DPPH: 2,2-diphenyl-1-picrylhydrazyl, TBA: Thiobarbituric acid, MDA: Malondialdehyde

1. Introduction

Kynurenic acid (4-Hydroxyquinoline-2-carboxylic acid; KYNA; Fig. 1A) is an endogenous substance that is formed from tryptophan via kynurenine metabolic pathway. However, KYNA is also present in dietary food products such as broccoli, potato, and spices (Turski, Turska, Kocki, Turski, & Paluszkiewicz, 2015; Turski, Turska, Zgrajka, Kuc, & Turski, 2009). The kynurenine metabolic pathway endogenously metabolizes tryptophan into KYNA, 3-hydroxykynurenine (3-HK) and quinolinic acid (QUIN) by kynurenine aminotransferase, kynurenine 3-monooxygenase, and kynureninase enzymes, respectively. The 3-HK is a potent free radical generator and QUIN acts as N-methyl-D-aspartate (NMDA) receptor agonist. However, KYNA is an ionotropic glutamate and alpha 7-nicotinic receptor antagonist (Vécsei, Szalárdy, Fülöp, & Toldi, 2013).

KYNA is an excitatory amino acid antagonist possessing neuroprotective properties. The neuroprotective effect of KYNA was demonstrated by László and beal (László & Beal, 1991). Carpenedo and co-workers showed the antagonistic activity of KYNA on glutamate receptors (Carpenedo et al., 2001). Several researchers have demonstrated the antioxidant and free radical scavenging properties of KYNA. KYNA is formed inside the central nervous system (CNS) and it is reported that KYNA is also present in human blood and peripheral organs. The decreased concentration of KYNA in the CNS is associated with several neurological disorders such as Parkinson's disease, multiple sclerosis and Huntington's disease (Schwarcz, Bruno, Muchowski, & Wu, 2013; Stone & Connick, 1985). However, low aqueous solubility and limited blood-brain barrier (BBB) permeability limits its therapeutic application (Hornok et al., 2012; Varga et al., 2016). Moreover, kynurenic acid itself has the ability to cross the blood-brain barrier (BBB) to a limited extent and accumulates in the brain on systemic administration (Stone, 2001). Moroni et

al. demonstrated that the concentration of KYNA in the mammalian brain is around 10 to 150 nM (Moroni, Russi, Lombardi, Beni, & Carlh, 1988). Several researchers have demonstrated the effect of KYNA upon systemic administration and its permeation across BBB. Varga et al. prepared KYNA loaded core-shell nanoparticles of bovine serum albumin (BSA) and demonstrated that peripheral administration of KYNA loaded BSA nanoparticles are sufficient enough to produce electrophysiological effects within the central nervous system (Varga et al., 2016). Hornok and co-workers prepared KYNA loaded micelles to demonstrate the pharmacological activity of KYNA on systemic administration (Hornok et al., 2012). Moreover, López et al. earlier demonstrated the synthesis of KYNA loaded silica nanoparticles to improve the solubilization of KYNA (López, Ortiz, Gómez, la Cruz, Verónica Pérez-de Carrillo-Mora, & Novaro, 2014). Different ester derivatives of KYNA were also prepared to improve its solubility and permeability (Dalpiaz et al., 2005).

Cyclodextrin-based delivery systems provide a promising platform to increase drug solubility, stability, and enhance the drug release profile. The inclusion complex of poorly water-soluble drugs with α-cyclodextrin, β-cyclodextrin, and γ-cyclodextrin is widely reported (A. Singh, Worku, & Mooter, 2011; Woldum, Larsen, & Madsen, 2008). However, there are certain drawbacks of native cyclodextrins such as small cavity size of α-cyclodextrin and γ-cyclodextrin is expensive. β-cyclodextrin is most commonly used in the drug delivery application nevertheless, β-cyclodextrin exhibits low aqueous solubility and nephrotoxicity (Challa, Ahuja, Ali, & Khar, 2006).

Several efforts have been made to overcome drawbacks associated with native cyclodextrins and, to improve their performance, different types of cyclodextrin nanosponges were prepared earlier. The nanosponges (NSs) are 3-dimensional hyper crosslinked polymer of native

cyclodextrins prepared with a variety of crosslinking agents such as 1,1'-carbonyldiimidazole (CDI), pyromellitic dianhydride (PMDA), and diphenyl carbonate (DPC) (Trotta, Dianzani, Caldera, Mognetti, & Cavalli, 2014; Venuti et al., 2017). Moreover, CDI based nanosponges are more stable at acidic and alkaline pH and comparatively low toxic to their other counterparts (Trotta, Zanetti, & Cavalli, 2012). Many researchers have also prepared modified nanosponges such as ionic β-cyclodextrin polymers (Berto et al., 2007) and glutathione responsive nanosponges (Trotta et al., 2016). Nanosponges have been utilized for a variety of applications such as enhancement of aqueous solubility and stability of nutraceuticals (Ansari, Vavia, Trotta, & Cavalli, 2011; Darandale & Vavia, 2013), encapsulation of proteins (Wajs, Caldera, Trotta, & Fragoso, 2013) and immobilization of enzymes (Di Nardo et al., 2009). It is also reported that cyclodextrins based nanocarriers facilitate the permeation of drug molecules across BBB on systemic administration (Shityakov et al., 2016). Furthermore, Cyclodextrin based NSs can be administered via several routes depending on the applications (Swaminathan et al., 2010; Torne, Darandale, Vavia, Trotta, & Cavalli, 2013).

In the present work, we demonstrated the synthesis and characterization of KYNA loaded cyclodextrin nanosponges. The enhancement in aqueous solubility, antioxidant activity, and in-vitro cell toxicity were also studied.

2. Materials and Method

2.1 Materials

The β-cyclodextrin was a kind gift from Roquette Italia (Cassano Spinola, Italy). Kynurenic acid, N,N'-carbonyldiimidazole, Thiobarbituric (TBA) acid and 2,2-diphenyl-1-picrylhydrazyl (DPPH) were purchased from Sigma-Aldrich (Milan, Italy). Cell culture reagents were

purchased from Gibco/Invitrogen (Life Technologies, Paisley, UK). All other chemicals and reagents used were of analytical grade unless otherwise specified.

2.2 Methods

2.2.1 Synthesis of β-cyclodextrin nanosponge (β-CDNS)

N,N'-carbonyldiimidazole (CDI) was used as a crosslinker to prepare β-cyclodextrin nanosponge as reported earlier by our group (Trotta et al., 2012). Briefly, β-cyclodextrin (β-CD) was dissolved in N,N-dimethylformamide (DMF) and CDI was added in a different molar ratio of 1:2, 1:4 and 1:6 resulting in the formation of three-different types of nanosponges. The reaction was carried out at 90 °C, in a magnetic stirrer for 3 hours that was continued overnight for further crosslinking. The solid monolithic mass of nanosponge was crushed and washed several times with water to remove unreacted components. The nanosponge was purified by Soxhlet extraction with ethanol (24 hours), air dried and stored in a desiccator at room temperature for further use. The nanosponges prepared with CDI were abbreviated as β-CDNS1, β-CDNS2, and, β-CDNS3 respectively.

The quantities of chemicals used in the synthesis of three-different types of nanosponges are listed in table 1.

Table 1.

Samples	Cyclodextrin (β-CD)		CDI		DMF	β-CD:CDI Molar Ratio
	(g)	(mmol)	(g)	(mmol)	(ml)	
β-CDNS1	5	4.405	1.426	8.794	30	2
β-CDNS2	5	4.405	2.852	17.588	30	4
β-CDNS3	5	4.405	4.278	26.382	30	6

2.2.2 Determination of swelling degree

All the nanosponges were dried overnight and known amounts of different nanosponges were placed in water. The swollen nanosponges were removed and excess of water was removed by blotting on filter paper. The weight of nanosponges was recorded and the above procedure was followed until a constant weight was achieved.

The following equation was used to calculate % swelling degree.

$$\% \text{ Swelling Degree} = \frac{\text{Weight in the swollen state} - \text{Weight in the dry state}}{\text{Weight in the dry state}} \text{ x } 100$$

2.2.3 Solubilization efficiency of nanosponges

The aqueous solubility of KYNA alone, with β-CD and with nanosponges (β-CDNS1 to β-CDNS3) was studied. An excess quantity of KYNA was suspended in water (2 ml) and a fixed quantity of β-CD or different nanosponges was added into it. The vials were placed on a mechanical shaker for 24 hours at room temperature. Later, the suspension was centrifuged at 6000 rpm for 15 minutes and the supernatant was collected. All the samples were filtered using a 0.45 µm syringe filter and analyzed on HPLC as mentioned in section 2.2.6.

2.2.4 Preparation of KYNA loaded nanosponge

KYNA loaded nanosponge was prepared by the freeze-drying method as established earlier (Zidan, Ibrahim, Afouna, & Ibrahim, 2018). An aqueous suspension of individual nanosponges (β-CDNS1 to β-CDNS3) was prepared (10 mg/ml) and the required quantity of KYNA was added into it at different weight ratio of 1:3, 1:4 and 1:5 (w/w), respectively. The suspension was sonicated for 10 minutes and stirred for 24 hours at room temperature. Later, the suspension was

centrifuged at 6000 rpm for 15 minutes to remove the non-complexed drug. The supernatant was collected, 5 % trehalose (% w/v) was added as a cryo-protectant and freeze-dried.

The freeze-dried formulations of KYNA were abbreviated as KYNA-β-CDNS1, KYNA-β-CDNS2, and KYNA-β-CDNS3, respectively.

2.2.5 Preparation of a physical mixture

Physical mixtures were also prepared by mixing drug (2.5 mg) with different nanosponges (10 mg) by trituration in a mortar for 30 min at room temperature. The physical mixture formulations were abbreviated as PM1, PM2, and PM3, respectively.

2.2.6 Quantitative determination of KYNA by HPLC

The quantitative determination of KYNA was performed by an HPLC system (PerkinElmer, Waltham, USA) equipped with a UV detector (Flexar UV/Vis LC spectrophotometer) using a phenomenex C18 analytical column (4.6 mm x 250 mm, 5 µm). The mobile phase consisted of a mixture of 0.14 % (v/v) TFA (trifluoroacetic acid) in water-acetonitrile (90:10 v/v), filtered and ultrasonically degassed prior to use. The mobile phase was pumped through the column at a flow rate of 1 ml/min and the samples (20 µl) were analyzed at 330 nm using a UV detector (Lesniak et al., 2013)

2.2.7 Determination of KYNA loading efficiency

The KYNA loaded NS was taken into a vial containing 1 ml of DMSO-water mixture (50:50) and sonicated for 1 hour. Later, it was filtered and suitably diluted with mobile phase and analyzed on HPLC.

2.2.8 Determination of particle size, polydispersity index, and zeta potential

The particle size and polydispersity index were studied by DLS using a Malvern Zetasizer Nano instrument at a fixed scattering angle of 90°. All the samples were suitably diluted by milli-Q water and analyzed at 25 °C. Zeta potential was calculated on the same instrument placing an additional electrode. All the measurements were performed in triplicate.

2.2.9 Differential Scanning Calorimetry (DSC)

Thermal properties of KYNA, blank NS, physical mixture, and KYNA loaded NS were evaluated using a TA instruments Q200 DSC (New Castle, DE, USA). The empty aluminum pan was used as a reference standard and samples (2-3 mg) were scanned from 30 to 300 °C at the scanning rate of 10 °C/min under a nitrogen purge.

2.2.10 Fourier transform infrared spectroscopy (FTIR)

The FTIR spectra of KYNA, blank NS, physical mixture, and KYNA loaded NS were recorded on PerkinElmer 100 FTIR using an attenuated total reflectance (ATR) accessory. All the samples were scanned from 4000-650 cm^{-1} at a resolution of 4 cm^{-1} and 8 scans/spectrum. The % crosslinking of nanosponges was also determined with some modifications as reported earlier (Coma, Sebti, Pardon, Pichavant, & Deschamps, 2003; Ghorpade, Yadav, & Dias, 2016). The detailed information of method and sample preparation is mentioned in the supplementary information.

2.2.11 X-ray powder diffraction studies (PXRD)

The XRD spectra of KYNA, blank NS and KYNA loaded NS were recorded using Malvern Panalytical X'Pert diffractometer using Cu Kα1 as a source of radiation. Data was collected over an angular range from 5 to 45 °2θ at a step size of 0.017 °2θ and a time per step of 100.33 s.

2.2.12 Morphology evaluation of nanosponge and drug complex

The surface morphologies of blank NS, and KYNA loaded NS were evaluated on Field Emission Scanning Electron Microscope (FE-SEM; ZIESS Supra 40). Approximately, 3-4 drops of NS suspension were placed on a copper stub and air dried later, sputter coated with gold. Samples were analyzed at 3 kV accelerating voltage at a working distance of 10 mm.

2.2.13 The in-vitro drug release profile

The accurate weight amount of KYNA loaded NS (20 mg) was dispersed in 3 ml of phosphate buffer pH 7.4 and sealed into a dialysis bag (12,400 MWCO). It was submerged into 30 ml of phosphate buffer pH 7.4 at 37 ± 0.5 °C in a rotation speed of 50 rpm. The aliquots (1 ml) were withdrawn at different time intervals and replaced with the same amount of fresh phosphate buffer to maintain sink condition. Later, all the samples were analyzed on HPLC.

2.2.14 Evaluation of antioxidant activity

2.2.14.1 TBA Assay

This assay is based on the oxidative decomposition of polyunsaturated fatty acid in acidic medium to generate malondialdehyde (MDA), which reacts with TBA to form TBA-MDA adduct (Yen, Chang, & Su, 2003). Two different concentrations (50 µM and 100 µM) of KYNA (1 mg/ml stock solution in N-methyl pyrrolidone) and KYNA loaded NS in phosphate buffer pH 7.4 were prepared. 0.1 ml of linoleic acid (1 % w/v) was taken in a test tube, 0.2 ml of sodium dodecyl sulfate (SDS) (4 % w/v), 1.5 ml of phosphoric acid (1.0 % v/v), 1.0 ml of TBA (0.6 % w/v), 0.1 ml of water and 0.1 ml of KYNA solution or KYNA loaded NS was added into it. The mixture was heated at 100 °C. 45 minutes later it was cooled down on an ice bath and mixed with 1-butanol (4 ml) to extract TBA-MDA adduct. Samples were analyzed by UV-Visible spectrophotometer (Lambda 25, PerkinElmer, Waltham, USA) at 535 nm and MDA

concentration was determined from a calibration curve of a MDA precursor 1,1,3,3-tetraethoxypropane (TRP), which was recorded under the same experimental conditions. The antioxidant activity of KYNA was evaluated by determining the reduction in the MDA generation.

The effect of potent oxidant ($KMnO_4$) on lipid peroxidation and its inhibition by KYNA or KYNA loaded NS was also studied using additional 0.1 ml of $KMnO_4$ (1 mM) solution following the procedure as mentioned above.

2.2.14.2 DPPH scavenging activity

The DPPH scavenging activity of KYNA loaded NS was studied and compared with the KYNA solution as demonstrated earlier (Colombo, Figueiró, Dias, Amanda de Fraga Teixeira, Battastini, & Koester, 2018). Different concentrations of KYNA and KYNA loaded NS (10-100 µM) were prepared. An ethanolic solution of DPPH (0.004 % w/v) was prepared, of which 0.5 ml were mixed with either KYNA solution or KYNA loaded NS (2 ml). Later, the mixture was incubated for 60 minutes and analyzed by UV-visible spectrophotometer at 525 nm. Ethanol (0.5 ml) was used as control (without drug) and results were compared with L-ascorbic acid as a positive standard. The percentage of DPPH scavenging activity was calculated using the following equation.

$$\text{DPPH Inhibition (\%)} = \frac{\text{Absorbance of control} - \text{Absorbance of sample}}{\text{Absorbance of control}} \text{ x } 100$$

2.2.14.3 H_2O_2 Scavenging activity

The H_2O_2 scavenging activity of KYNA and KYNA loaded NS was evaluated as reported earlier (Ebadollahinatanzi & Moghadasi, 2016). Briefly, a series of concentrations of KYNA and KYNA loaded NS (10-100 µM) were prepared. The reaction was carried out between 0.5 ml of

KI (1M), 0.5 ml of TCA (0.1% w/v), 0.5 ml of phosphate buffer pH 7.4, 0.5 ml of H_2O_2 (10 mM) and KYNA or KYNA loaded NS (0.5 ml) at room temperature for 10 minutes. The phosphate buffer pH 7.4 (0.5 ml) was added instead of drug solution as a control. The absorbance was recorded by UV-Vis spectrophotometer at 350 nm.

The following equation was used to calculate the percentage of H_2O_2 scavenging activity.

$$H_2O_2 \text{ Scavenging Activity } (\%) = \frac{\text{Absorbance of control} - \text{Absorbance of sample}}{\text{Absorbance of control}} \text{ x } 100$$

2.2.15 Cell viability studies

SHSY-5Y human neuroblastoma cell lines were purchased from ATCC (Manassas, VA, USA). The cells were cultured as a monolayer in RPMI 1640 medium accompanied with 10 % fetal calf serum, 100 U/ml penicillin, and 100 µg/ml streptomycin at 37 ℃ and maintained under 5 % CO_2 atmosphere. The cell viability of KYNA, KYNA loaded NS and blank NS was evaluated by 3-(4,5-dimethylthiazol-2-yl)-2,5-diphenyltetrazolium bromide (MTT) assay.

SHSY-5Y cell lines were seeded into a 96-well plate and incubated for 24 hours at 37 ℃ in a 5 % CO_2 humidified atmosphere. The cells were incubated with increasing concentrations of KYNA or KYNA loaded NS (1-100 µM) for 24 hours. The Blank NS was also dispersed in 0.9 % NaCl saline solution and treated with the cells as mentioned above. After 24 hours, cell viability was evaluated using MTT by recording the absorbance at 570 nm according to the manufacturer's protocol. The cells treated with culture medium alone considered as a control and the reading obtained from treated cell were expressed as % cell viability.

290 **2.2.16 Stability study of KYNA loaded NS**

291 The in vitro stability of blank NS and KYNA loaded NS in 0.9 % NaCl saline solution was

292 evaluated. All the samples were incubated at 4 °C for a period of 1 week. The average diameter

293 and zeta potential of blank NS and KYNA loaded NS were studied at different time intervals.

294 **2.2.17 Statistical analysis**

295 The experiments are expressed as mean ± standard deviation (SD). The significance of the

296 difference was evaluated by one-way ANOVA followed by Bonferroni correction using

297 GraphPad Prism 5 software (GraphPad Software, USA). A p-value < 0.05 was considered as

298 statistically significant.

299 # 3. Results and discussion

300 **3.1 Physicochemical Characterization of NS and KYNA loaded NS**

301 The presence of a large number of hydroxyl groups of β-CD makes it a suitable candidate for

302 the crosslinking reaction. The nanosponges were synthesized by the formation of a carbonate

303 bond between CDI and the hydroxyl groups of β-CD. The swelling degree of the prepared NS

304 was determined. A moderate swelling degree was achieved with β-CDNS2 (251 %), compared to

305 β-CDNS1 (200 %) and β-CDNS3 (168 %). However, no evident trend was observed.

306

(A) **(B)**

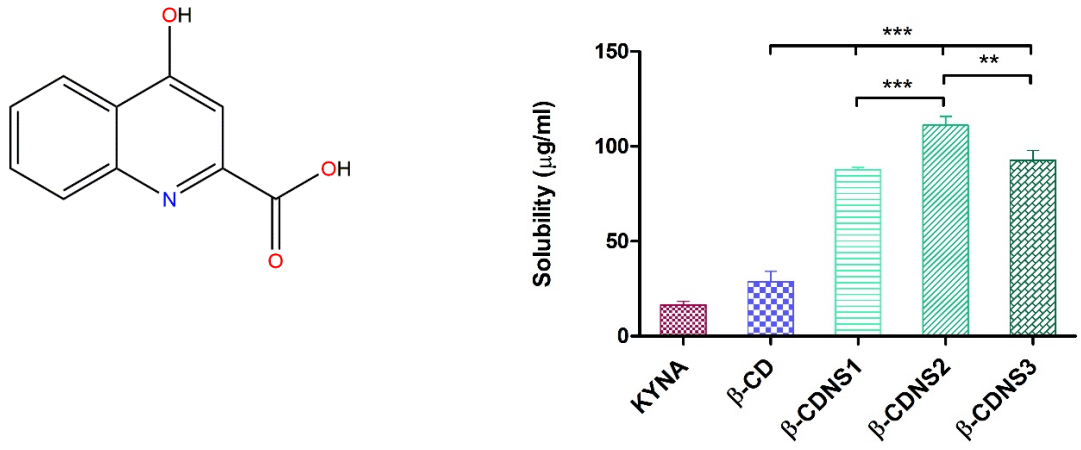

Figure 1.

The solubilization of KYNA alone and in the presence of β-CD or different nanosponges was also studied as presented in Fig. 1(B). The solubility of KYNA with different nanosponges was significantly higher compared to both free KYNA (16.4 µg/ml) and KYNA with β-CD (28.6 µg/ml). The solubility of KYNA increased to 5.3 folds with β-CDNS1 and 6.77 folds with β-CDNS2. However, KYNA solubility further decreased with β-CDNS3 (5.65 folds) because of the higher cross-linker concentration that formed more complex nanochannel which hindered the drug encapsulation (Torne et al., 2013). The maximum solubilization of KYNA was achieved with β-CDNS2 (Fig. S1; Supporting Information), thus β-CDNS2 was selected for drug loading studies.

Later, drug loading study was carried by taking different KYNA to β-CDNS2 concentrations in weight ratios of 1:3, 1:4 and 1:5 w/w. The maximum drug loading of 19.06 % was achieved with 1:4 w/w compared to 12.7 % (1:3 w/w) and 19.19 % (1:5 w/w), respectively. A significant difference in drug loading was observed in between 1:3 w/w and 1:4 w/w. However, no further

change in drug loading was seen in between 1:4 w/w and 1:5 w/w might be due to saturation solubility of KYNA (Zidan et al., 2018).

Depending on the drug loading studies KYNA loaded NS (1:4 w/w) subjected to further studies. The average particles size and zeta potential of blank nanosponge and KYNA loaded NS were determined as shown in Table 2.

Table 2.

Properties	Blank NS (β-CDNS2)	KYNA loaded NS (KYNA-β-CDNS2)
Particle Size (nm)	224.43 ± 3.72	255.8 ± 7.88
PDI	0.35 ± 0.040	0.32 ± 0.043
Zeta Potential (mV)	-26.3 ± 1.91	-23 ± 0.945
Encapsulation Efficiency (%)	-	95.31 %

The DSC thermogram of KYNA showed an endothermic peak at 277.15 °C that corresponds to its melting temperature as shown in Fig. 2(I). The nanosponges are stable thus do not undergo any thermal transition and physical mixture showed endothermic transition similar to KYNA with lesser intensity because of the possible dilution with NS. It is reported that encapsulation of drug molecules within the NS leads to the formation of an amorphous system (Ansari et al., 2011). A similar pattern was observed with KYNA loaded NS which did not produce any significant endothermic melting because of possible amorphization of KYNA, thus confirming the encapsulation of KYNA within the nanosponges.

Fig. 2(II) shows the FTIR spectra of KYNA, blank NS, physical mixture and KYNA loaded NS. The FTIR spectrum of KYNA showed strong characteristic peaks at 3095 cm^{-1} (-N-H stretching), 2940 cm^{-1} (-C-H stretching), 1660 cm^{-1} (-C=C stretching), 1362 cm^{-1} (-OH bending), 1121 cm^{-1} (-C-O stretching). The occurrence of carbonate bond peak at 1739 cm^{-1} in the FTIR spectrum is the characteristic feature of NS (Lembo et al., 2013).

(I) **(II)**

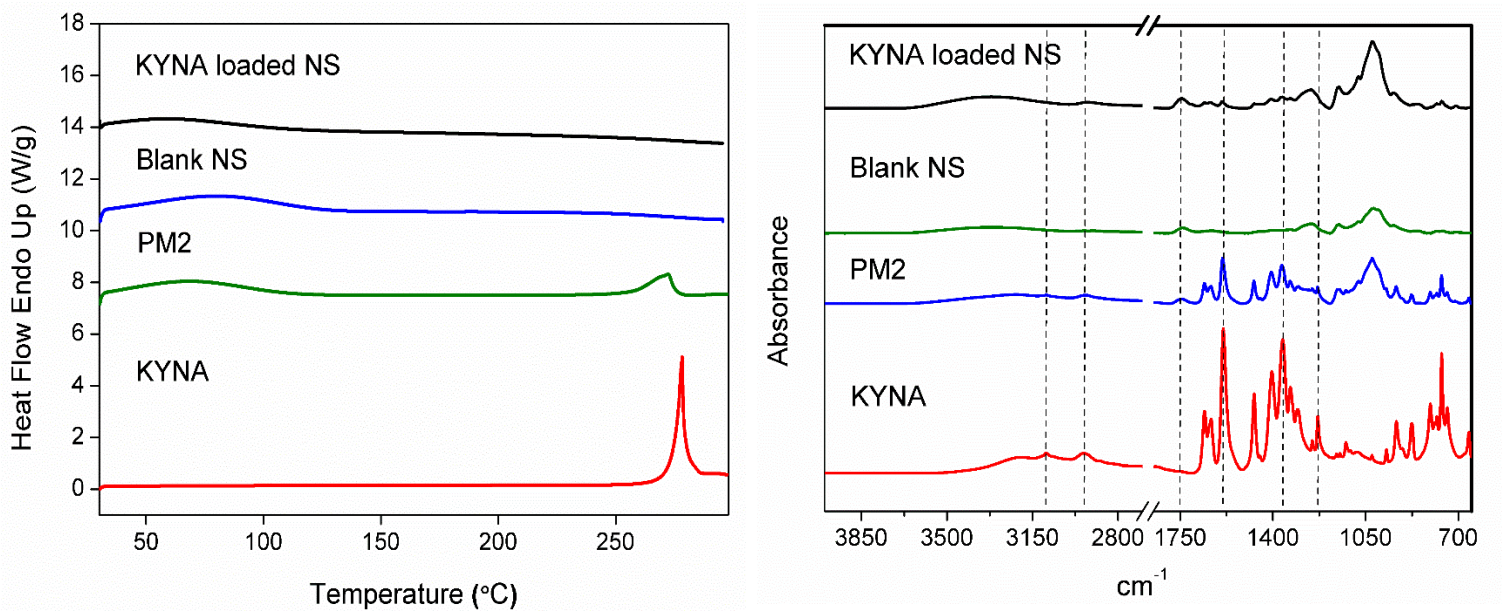

(III) **(IV)**

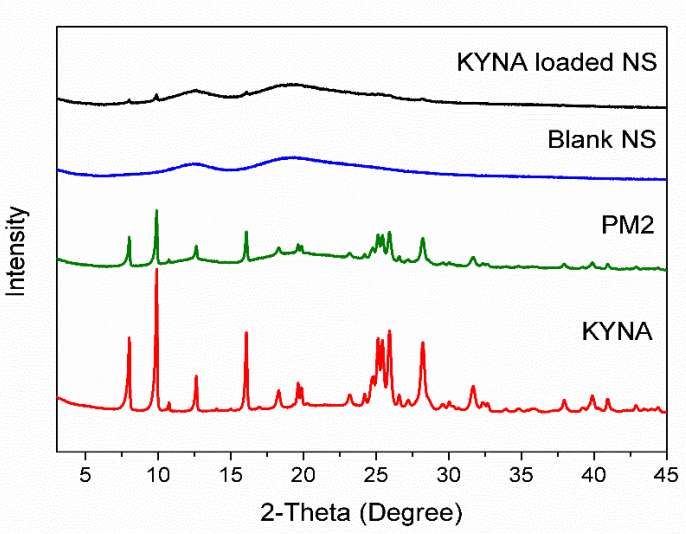

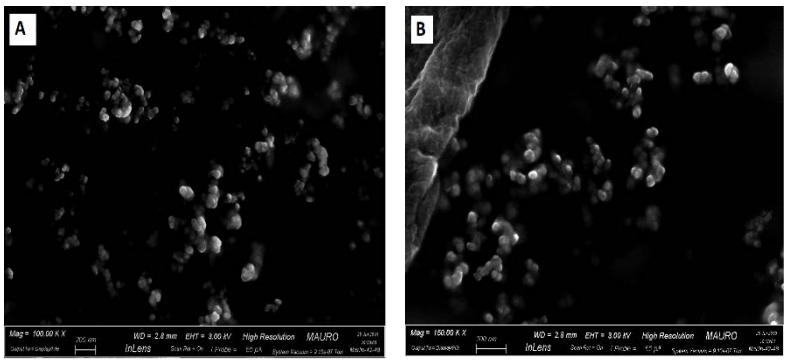

Figure 2.

Moreover, FTIR spectrum of the physical mixture showed the superposition of FTIR peaks of both KYNA and NS without any shift or suppression, confirming no interaction or encapsulation of KYNA with NS. However, the FTIR spectrum of KYNA loaded NS showed the disappearance of peaks at 3095 cm^{-1} (-N-H stretching), and a significant shift in the absorption band at 3318 cm^{-1} (-OH stretching), and 1743 cm^{-1} (-C=O stretching) indicating the interaction of KYNA with NS because of the possible encapsulation of drug. The extent of crosslinking of nanosponges was determined from the ratio of the two peaks (I_{1774}/I_{2929}) which corresponds to the carbonyl group stretching of the crosslinker and C-H stretching of β-CD, respectively. It was observed that the high ratio of I_{1774}/I_{2929} was obtained by increasing the crosslinker concentration due to increment in the I_{1774} band of the carbonyl group (Table S1; Supporting Information). It

suggested that higher crosslinker concentration leads to higher crosslinking of the nanosponges. β-CDNS1 showed lowest crosslinking of 59.49 % compared to β-CDNS2 (79.42 %) and β-CDNS3 (83.7 %) (Fig. S2-S4; Supporting Information). The % crosslinking values were similar to those reported earlier for other cyclodextrins nanosponges (Gholibegloo et al., 2019; P. Singh et al., 2018).

The PXRD pattern of KYNA showed sharp and intense peaks at 8.01, 9.90, 12.62, 16.07, 24.79, 28.22, 31.68, and 39.89 2θ values that indicates crystalline behavior of KYNA as shown in Fig. 2(III). The PXRD of blank NS did not show any sharp peaks in agreement with its amorphous nature. The disappearance of characteristic peaks of KYNA in KYNA loaded NSs indicate a loss in the crystallinity and consequent amorphization of KYNA because of the encapsulation of KYNA inside the NSs. Such evidence suggested the formation of an inclusion complex (Darandale & Vavia, 2013; Dora et al., 2016). However, in case of physical mixture characteristic peaks of KYNA were clearly visible with lesser intensity, suggesting no change in the property of KYNA, which remained in the crystalline form. The PXRD pattern of β-CD was also determined and the presence of sharp peaks clearly indicated crystalline structure of it in contrast to the NSs (Fig. S5; Supporting Information).

(A) **(B)**

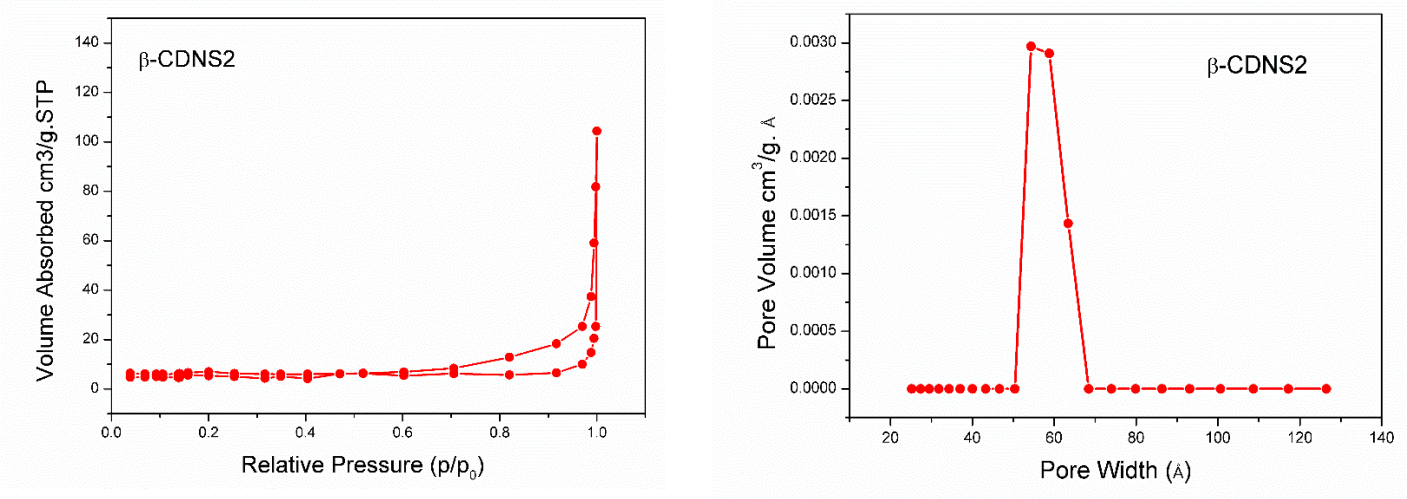

Figure 3.

Fig. 2(IV) shows the FE-SEM images of blank NS and KYNA loaded NS in which both showed small spherical shape particles of diameter less than 200 nm with appropriate size distribution. Furthermore, fig. 3 presents the N_2 adsorption-desorption isotherm and pore distribution curve of blank NS. As shown in fig. 3(A), a type IV isotherm with hysteresis loop was observed for NS. The presence of hysteresis loop could be attributed to the mesoporous structure of the NS. Moreover, fig. 3(B) displayed the pore distribution of NS which further suggest the mesoporosity of NS as the pore diameter was 50-70 Å (5-7 nm). The surface area of blank NS was less than 1 m^2/g. It is also reported that the surface area and porosity can be tailored depending upon the cross-linker concentration. The results obtained were in agreement with those previously reported in the literature for other cyclodextrin nanosponges (Gholibegloo et al., 2019; Pushpalatha, Selvamuthukumar, & Kilimozhi, 2018). Moreover, BET analysis of KYNA loaded NS showed a type IV isotherm with hysteresis loop similar to blank NS. However, porosity of KYNA loaded NS (35-45 Å) was reduced which might be due to encapsulation of KYNA within the NSs (Fig. S6; Supporting Information).

The in-vitro release profile of KYNA loaded NS was studied in phosphate buffer pH 7.4 (Fig. 4). A slow and uniform drug release profile of KYNA was observed without any initial burst effect. The slower drug release profile can be attributed to the presence of KYNA inside the cavities of nanosponges. Moreover, the absence of an initial burst release further confirmed that the drug was not partially encapsulated or adsorbed on the surface of nanosponges. The different drug release kinetics models (such as zero order, first order, Higuchi-Connors, Hixen-Crowell, and Korsmeyer-Peppas) were applied and the release profile of KYNA was best fitted to Higuchi-Connors release kinetic model (R^2 = 0.995) indicating that drug release was carried out by diffusion from the nanosponges (Machín, Isasi, & Vélaz, 2012; Zainuddin, Zaheer, Sangshetti, & Momin, 2017).

Plain KYNA was found to be dissolved very rapidly and uncontrolled release was observed. Plain KYNA showed that equilibrium was achieved within a few minutes during in-vitro release profile. Moreover, rapid drug release is associated with dose related toxic effects. Therefore, controlled drug delivery, which can be achieved by encapsulation of drug within NSs, is required (Wen, Jung, & Li, 2015).

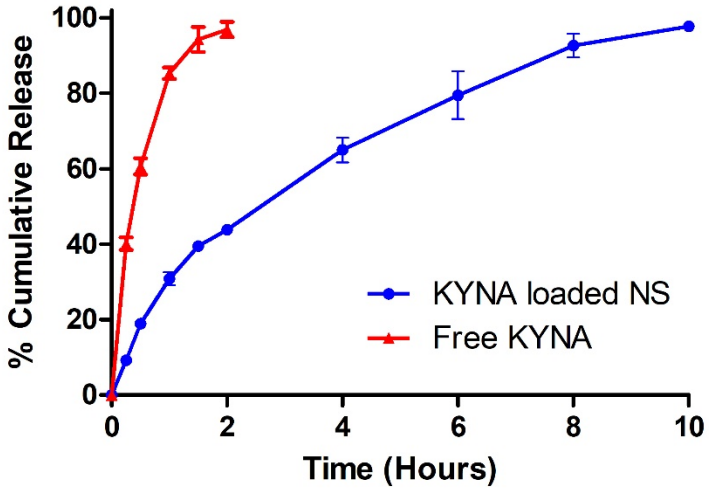

Figure 4.

3.2 Evaluation of antioxidant activity

Phenolic compounds exhibit antioxidant activity because of their ability to react with free radicals at a faster rate. The antioxidant activity of KYNA might be because of the presence of an aromatic hydroxyl group that readily provides protons for the reaction with free radicals. Moreover, the presence of nitrogen in the aromatic ring or carboxylic acid acting as an electron withdrawing group helps to stabilize the free radical produced by donation of the proton (Zhuravlev, Zakharov, Shchegolev, & Savvateeva-Popova, 2016).

The generation of MDA because of the degradation of fatty acid is a common indicator for determining the degree of lipid peroxidation. MDA reacts with TBA to produce a pink TBA-MDA adduct. The production of MDA is shown in fig. 5 and it was observed that KYNA loaded NS produced a lesser amount of MDA ($P<0.001$) compared to free KYNA. A decreased production of MDA might be because of the inhibiting and scavenging effect of KYNA on ROS produced during oxidation process.

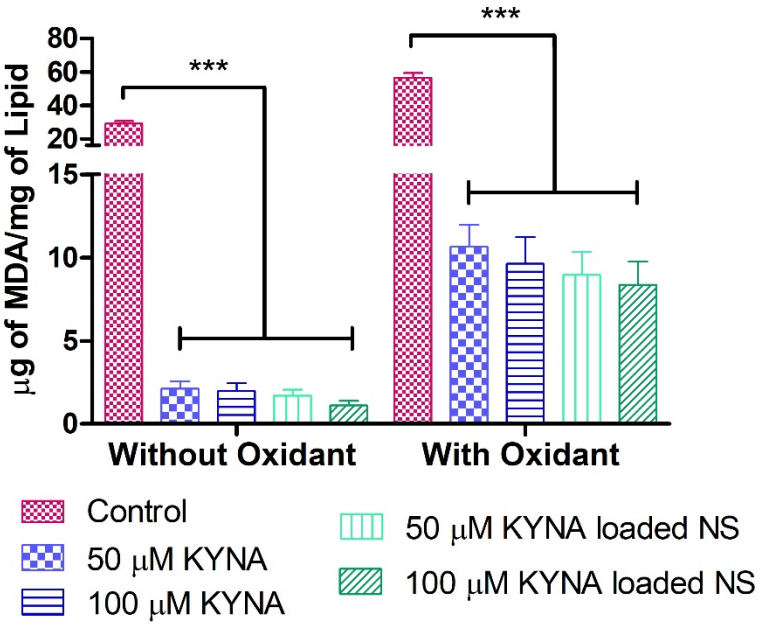

Figure 5.

The effect of KYNA on MDA generation in the presence of the strong oxidizing agent (i.e. $KMnO_4$) was also studied and it was observed that oxidizing agent generated a large amount of MDA because of the rapid and higher oxidation of fatty acid. However, free KYNA and KYNA loaded NS significantly decreased the production of MDA even in the presence of the oxidizing agent, demonstrating its antioxidant potential. Moreover, KYNA loaded NS was more effective compared to free KYNA, this might be because of the higher solubilization of KYNA with NS.

The DPPH assay is based on the reduction of its absorbance at 517 nm because of the acceptance of proton. Fig. 6(A) illustrates the DPPH inhibition effect of KYNA at different concentrations. It was observed that the DPPH inhibition effect of KYNA was increased in a dose-dependent manner. Moreover, the KYNA loaded NS showed a higher reduction ($P<0.001$) in the DPPH concentration compared to free KYNA at higher concentration.

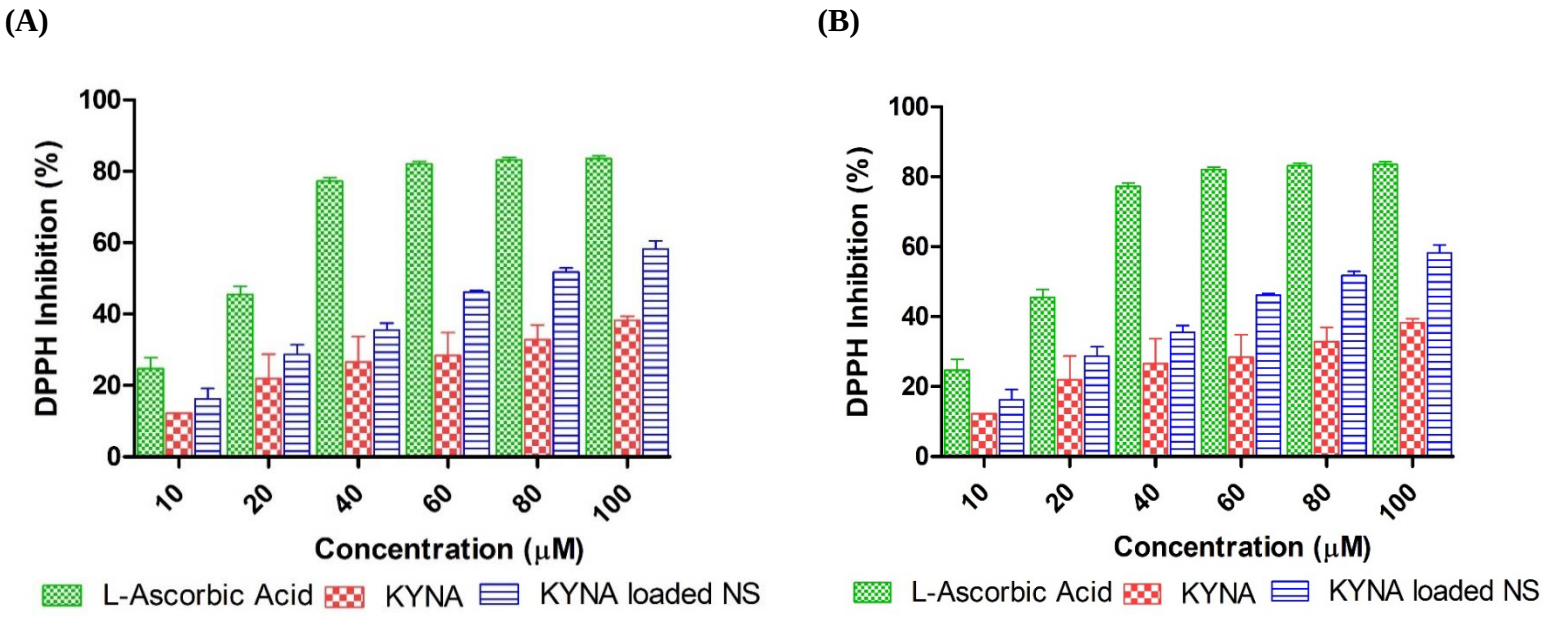

Figure 6.

The higher antioxidant activity of KYNA loaded NS can be attributed to enhanced solubilization of KYNA with nanosponge thus readily provided protons to DPPH. The results obtained are in agreement with those reported in the literature. Sundararajan et al. demonstrated that chrysin loaded NS produced more than 2 fold DPPH inhibition compared to free chrysin. (Sundararajan, Thomas, Venkadeswaran, Jeganathan, & Geraldine, 2017).

Moreover, the antioxidant property of KYNA was further evaluated by hydrogen peroxide scavenging activity. The hydrogen peroxide is a very reactive compound that generates hydroxyl radicals. The hydroxyl radicals are the most common reactive oxygen species (ROS) that can cause cell death because of the oxidative degradation of biomolecules such as DNA, RNA, and proteins. Thus, to demonstrate the antioxidant potential of KYNA, its H_2O_2

scavenging effect was studied. Fig. 6(B), shows the hydrogen peroxide scavenging effect of KYNA, KYNA loaded NS and L-ascorbic acid.

All the samples showed concentration-dependent H_2O_2 inhibition. The KYNA loaded NS showed better H_2O_2 inhibition compared to free KYNA ranging from 17 % to 78 % at the tested concentration range. It might be possible that KYNA loaded NS reacts rapidly with peroxide intermediates to exhibit better H_2O_2 inhibition due to high KYNA solubilization. It is also evident that the standard solution of L-ascorbic acid is more effective compared to KYNA and KYNA loaded NS. The above-mentioned tests were also carried out on blank NS to determine the antioxidant activity of NS alone. However, no significant results were obtained as they do not exhibit antioxidant activity (Fig. S7; Supporting Information).

The results observed are in agreement with those reported in the literature. Lugo-Huitrón et al. demonstrated the scavenging capacity of KYNA compared to known reference compounds and suggested that KYNA acts as a potent inhibitor of ROS (Lugo-Huitrón et al., 2011). In another study, Genestet and co-workers demonstrated the superoxide scavenging activity of KYNA. They demonstrated that KYNA showed better antioxidant activity compared to other tryptophan metabolites (Genestet et al., 2014).

3.3 Cell Viability

The biocompatibility of SHSY-5Y cell lines with blank NS was determined using a MTT assay at the concentration of 5-500 µg/ml indicated that blank nanosponge does not produce any significant toxic effect even at higher concentration thus confirming the safety of our nanocarrier (fig. 7). The minimum cell viability was 89 % at the concentration of 500 µg/ml after 24 hours. The results obtained are in agreement with previously reported data indicating that NS does not

produce any significant toxicity on different cell lines (Gholibegloo et al., 2019; Mognetti et al., 2012).

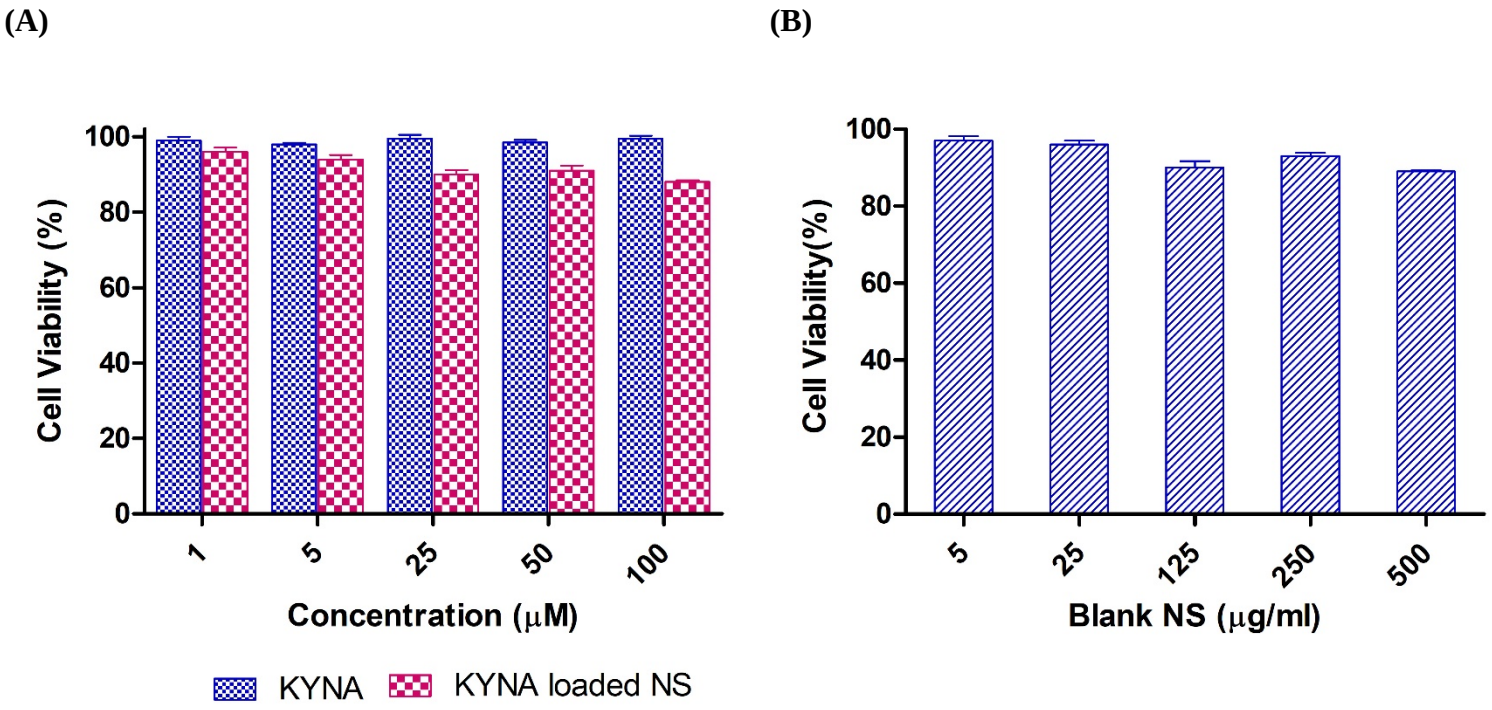

Figure 7.

The effect of KYNA and KYNA loaded NS was also evaluated on the survival of SHSY-5Y cell lines. Both KYNA and KYNA loaded NS do not produce any significant toxic effects on cell lines at the concentration of 1-100 µM. Furthermore, 90 % or more cell survival was observed at all the tested concentrations with KYNA and KYNA loaded NS. Klein et al. earlier demonstrated the effect of KYNA and its derivatives on the survival of SHSY-5Y cell lines which suggested that KYNA promotes higher cell survival of SHSY-5Y cell lines compared to the structurally modified derivative of KYNA (Klein et al., 2013). Researchers have also tried to prepare water-soluble salts of KYNA to improve the performance in the neurological applications. However, selectivity and stability of salts of KYNA are always the major concerns. Dalpiaz et al., prepared

6-bromo-ascorbic acid derivative of KYNA and reported that it showed the affinity to the vitamin C transporters, however, does not show any permeation because of the enzymatic hydrolysis (Dalpiaz et al., 2005). In another study Baron et al., prepared a KYNA analog and showed that higher concentration of KYNA analog was needed to produce glutamate inhibition compared to native KYNA (Baron et al., 1992). It suggested that native KYNA shows better neurological effects compared to its derivatives, therefore, NSs can be employed as a delivery vehicle for KYNA without any undesirable effects.

3.4 Stability study

The stability of blank NS and KYNA loaded NS was evaluated at 4 °C for a week. The particle size and zeta potential were studied to assess the stability of the blank NS and KYNA loaded NS. The change in the particle size and zeta potential is demonstrated in fig. 8(A) and 8(B), respectively.

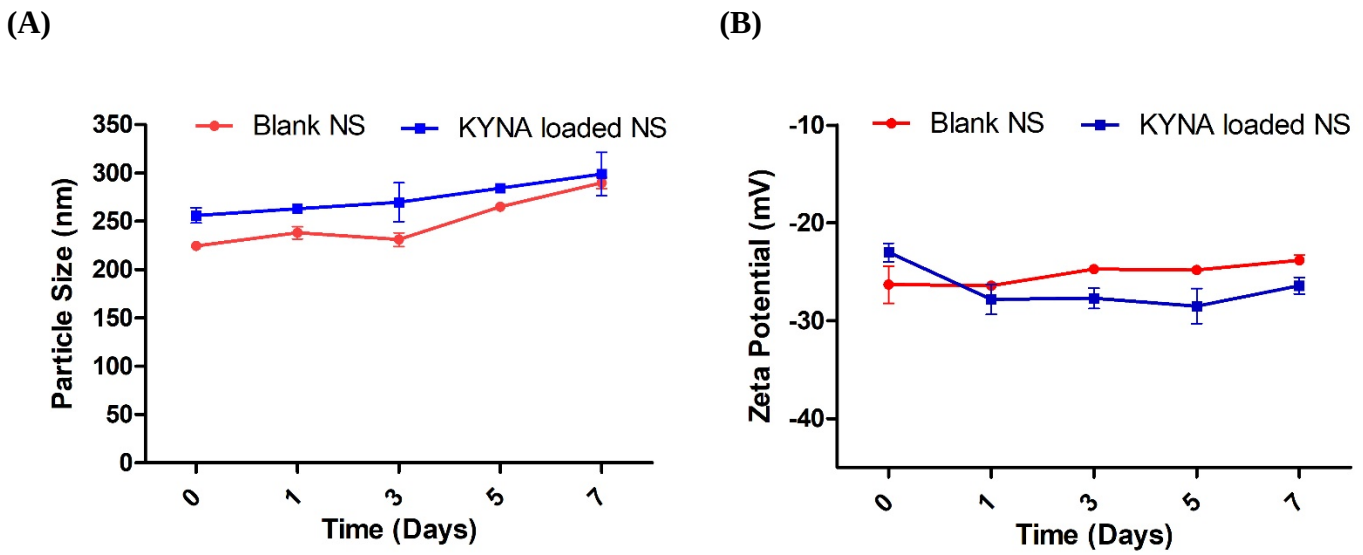

Figure 8.

It was observed that the particle size of blank NS was increased from 224.4 nm to 289.7 nm compared to KYNA loaded NS that showed a slight increase from 255.8 nm to 298.8 nm. Moreover, the zeta potential was also observed in the desired range without any significant change. Argenziano et al. earlier demonstrated that particle size of drug loaded NSs do not show any significant increment on storage for 24 hours (Argenziano et al., 2018). However, another study revealed that other hyper cross-linked polymer of cyclodextrin showed more than 2-fold increment in the particles size on storage within a week (Gref et al., 2006). On the basis of the above results, it is clear that these NSs provide better protection from aggregation and remained stable for the period of a week at 4 ℃.

4. Conclusion

In the present study, we demonstrated the synthesis of KYNA loaded NS and it was observed that high solubilization and drug loading of KYNA was achieved with β-CDNS2. The higher solubilization of KYNA was obtained because of the encapsulation of KYNA in the cyclodextrin cavities and porous matrix of NS. The KYNA loaded NS was characterized by FTIR, DSC, and PXRD which confirmed the formation of an inclusion complex of KYNA with NS. The antioxidant potential of KYNA and KYNA loaded NS was studied which further confirmed that KYNA loaded NS shows better antioxidant activity compared to free KYNA which can be attributed to the change in the physiochemical property and higher solubilization of KYNA with NS. The cytotoxicity of KYNA and KYNA loaded NS was also evaluated on SHSY-5Y cell lines which demonstrated that KYNA alone and in the presence of NS does not produce any significant toxic effect. Moreover, nanosponge alone was found to be non-toxic. Thus, the above study demonstrated that cyclodextrin nanosponge acts as a promising carrier for

the delivery of KYNA and can possibly be employed in biological systems for its antioxidant potential.

Conflict of interest

The authors declare no conflict of interest.

Acknowledgments

We would like to thank the University of Turin (ex-60 %) for providing the funds and Roquette Italia for their support.

Figure Captions

Fig 1. (A) Structure of KYNA. (B) Solubilization efficiency of KYNA, β-CD and different nanosponges. All the values present data in triplicate (mean ± SD); * indicates $P < 0.05$ and *** indicates $P < 0.0001$.

Fig 2. (I) DSC thermograms of KYNA, physical mixture, blank NS and KYNA loaded NS. (II) FTIR spectra of KYNA, physical mixture, blank NS and KYNA loaded NS. (III) PXRD pattern of KYNA, physical mixture, blank NS and KYNA loaded NS. (IV) FE-SEM images of blank NS (A), and KYNA loaded NS (B) (scale bar = 200 nm).

Fig 3. N_2 absorption-desorption (A) and porosity curve of β-CDNS2 (B).

Fig 4. In-vitro release kinetics of KYNA from NS.

Fig 5. The inhibition of lipid peroxidation by KYNA loaded NS in the absence of oxidizing agent (left) and in the presence of the oxidizing agent (right). Statistical significance *** indicates $P < 0.0001$.

Fig 6. The Percentage DPPH inhibition (A) and H_2O_2 scavenging activity (B) by KYNA, KYNA loaded NS and L-ascorbic acid.

Fig 7. The evaluation of in-vitro cytotoxicity study of KYNA and KYNA loaded NS (A) and blank NS (B) on SHSY-5Y cell lines after 24 hours.

Fig 8. The in-vitro stability study of blank NS and KYNA loaded NS to determine particles size (A) and zeta potential (B). All the values present in terms of mean ± SD (n = 3).

Table Captions

Table 1. Quantities of chemicals used for preparing nanosponges.

Table 2. Physicochemical characteristics of Blank and KYNA loaded NS.

References

Ansari, K. A., Vavia, P. R., Trotta, F., & Cavalli, R. (2011). Cyclodextrin-Based Nanosponges for Delivery of Resveratrol: In Vitro Characterisation, Stability, Cytotoxicity and Permeation Study. *AAPS PharmSciTech*, *12*(1), 279–286. https://doi.org/10.1208/s12249-011-9584-3.

Argenziano, M., Lombardi, C., Ferrara, B., Trotta, F., Caldera, F., Blangetti, M., Cavalli, R. (2018). Glutathione/pH-responsive nanosponges enhance strigolactone delivery to prostate cancer cells. *Oncotarget*, *9*(88), 35813–35829. https://doi.org/10.18632/oncotarget.26287.

Baron, B. M., Harrison, B. L., McDonald, I. A., Meldrum, B. S., Palfreyman, M. G., Salituro, F. G., White, H. S. (1992). Potent indole- and quinoline-containing N-methyl-D-aspartate antagonists acting at the strychnine-insensitive glycine binding site. *J Pharmacol Exp Ther*, *262*(3), 947–956.

Berto, S., Bruzzoniti, M. C., Cavalli, R., Perrachon, D., Prenesti, E., Sarzanini, C., Tumiatti, W. (2007). Synthesis of new ionic β-cyclodextrin polymers and characterization of their heavy metals retention. *Journal of Inclusion Phenomena and Macrocyclic Chemistry*, *57*(1–4), 631–636. https://doi.org/10.1007/s10847-006-9273-0.

Carpenedo, R., Pittaluga, A., Cozzi, A., Attucci, S., Galli, A., Raiteri, M., & Moroni, F. (2001). Presynaptic kynurenate-sensitive receptors inhibit glutamate release. *European Journal of Neuroscience*, *13*, 2141–2147. https://doi.org/10.1046/j.0953-816x.2001.01592.x.

Challa, R., Ahuja, A., Ali, J., & Khar, R. K. (2006). Cyclodextrins in drug delivery: An updated review. *AAPS PharmSciTech*, *6*(2), E329–E357. https://doi.org/10.1208/pt060243.

Colombo, M., Figueiró, F., Dias, Amanda de Fraga Teixeira, H. F., Battastini, A. M. O., &

566 Koester, L. S. (2018). Kaempferol-loaded mucoadhesive nanoemulsion for intranasal
567 administration reduces glioma growth in vitro. *International Journal of Pharmaceutics*, *543*(1–
568 2), 214–223. https://doi.org/10.1016/j.ijpharm.2018.03.055.

569 Coma, V., Sebti, I., Pardon, P., Pichavant, F. H., & Deschamps, A. (2003). Film properties from
570 crosslinking of cellulosic derivatives with a polyfunctional carboxylic acid. *Carbohydrate*
571 *Polymers*, *51*(3), 265–271. https://doi.org/10.1016/S0144-8617(02)00191-1.

572 Dalpiaz, A., Pavan, B., Vertuani, S., Vitali, F., Scaglianti, M., Bortolotti, F., Manfredini, S.
573 (2005). Ascorbic and 6-Br-ascorbic acid conjugates as a tool to increase the therapeutic effects of
574 potentially central active drugs. *European Journal of Pharmaceutical Sciences*, *24*(4), 259–269.
575 https://doi.org/10.1016/j.ejps.2004.10.014.

576 Darandale, S. S., & Vavia, P. R. (2013). Cyclodextrin-based nanosponges of curcumin:
577 Formulation and physicochemical characterization. *Journal of Inclusion Phenomena and*
578 *Macrocyclic Chemistry*, *75*(3–4), 315–322. https://doi.org/10.1007/s10847-012-0186-9.

579 Di Nardo, G., Roggero, C., Campolongo, S., Valetti, F., Trotta, F., & Gilardi, G. (2009).
580 Catalytic properties of catechol 1,2-dioxygenase from Acinetobacter radioresistens S13
581 immobilized on nanosponges. *Dalton Transactions*, *2*(33), 6507–6512.
582 https://doi.org/10.1039/b903105g.

583 Dora, C. P., Trotta, F., Kushwah, V., Devasari, N., Singh, C., Suresh, S., & Jain, S. (2016).
584 Potential of erlotinib cyclodextrin nanosponge complex to enhance solubility, dissolution rate, in
585 vitro cytotoxicity and oral bioavailability. *Carbohydrate Polymers*, *137*, 339–349.
586 https://doi.org/10.1016/j.carbpol.2015.10.080.

587 Ebadollahinatanzi, A., & Moghadasi, H. (2016). Hydrogen peroxide scavenging activity of two

different infusions made from black tea. *Toxicology Letters*, *258*, S192–S193. https://doi.org/10.1016/j.toxlet.2016.06.1706.

Genestet, C., Le Gouellec, A., Chaker, H., Polack, B., Guery, B., Toussaint, B., & Stasia, M. J. (2014). Scavenging of reactive oxygen species by tryptophan metabolites helps Pseudomonas aeruginosa escape neutrophil killing. *Free Radical Biology and Medicine*, *73*, 400–410. https://doi.org/10.1016/j.freeradbiomed.2014.06.003.

Gholibegloo, E., Mortezazadeh, T., Salehian, F., Ramazani, A., Amanlou, M., & Khoobi, M. (2019). Improved curcumin loading, release, solubility and toxicity by tuning the molar ratio of cross-linker to β-cyclodextrin. *Carbohydrate Polymers*, (213), 70–78. https://doi.org/10.1016/j.carbpol.2019.02.075.

Ghorpade, V. S., Yadav, A. V., & Dias, R. J. (2016). Citric acid crosslinked cyclodextrin/hydroxypropylmethylcellulose hydrogel films for hydrophobic drug delivery. *International Journal of Biological Macromolecules*, *93*, 75–86. https://doi.org/10.1016/j.ijbiomac.2016.08.072.

Gref, R., Amiel, C., Molinard, K., Daoud-Mahammed, S., Sébille, B., Gillet, B., Couvreur, P. (2006). New self-assembled nanogels based on host-guest interactions: Characterization and drug loading. *Journal of Controlled Release*, *111*(3), 316–324. https://doi.org/10.1016/j.jconrel.2005.12.025.

Hornok, V., Bujdosó, T., Toldi, J., Nagy, K., Demeter, I., Fazakas, C., Dékány, I. (2012). Preparation and properties of nanoscale containers for biomedical application in drug delivery: Preliminary studies with kynurenic acid. *Journal of Neural Transmission*, *119*(2), 115–121. https://doi.org/10.1007/s00702-011-0726-2.

Klein, C., Patte-mensah, C., Taleb, O., Bourguignon, J., Schmitt, M., Bihel, F., Mensah-nyagan, A. G. (2013). The neuroprotector kynurenic acid increases neuronal cell survival through neprilysin induction. *Neuropharmacology*, *70*, 254–260. https://doi.org/10.1016/j.neuropharm.2013.02.006.

László, V., & Beal, M. F. (1991). Comparative behavioral and pharmacological studies with centrally administered kynurenine and kynurenic acid in rats. *European Journal of Pharmacology*, *196*(3), 239–246. https://doi.org/10.1016/0014-2999(91)90436-T.

Lembo, D., Swaminathan, S., Donalisio, M., Civra, A., Pastero, L., Aquilano, D., Cavalli, R. (2013). Encapsulation of Acyclovir in new carboxylated cyclodextrin-based nanosponges improves the agent's antiviral efficacy. *International Journal of Pharmaceutics*, *443*(1–2), 262–272. https://doi.org/10.1016/j.ijpharm.2012.12.031.

Lesniak, W. G., Jyoti, A., Mishra, M. K., Louissaint, N., Romero, R., Chugani, D. C., Kannan, R. M. (2013). Concurrent quantification of tryptophan and its major metabolites. *Anal Biochem*, *443*(2), 222–231. https://doi.org/10.1016/j.ab.2013.09.001.Concurrent.

López, T., Ortiz, E., Gómez, E., la Cruz, Verónica Pérez-de Carrillo-Mora, P., & Novaro, O. (2014). Preparation and Characterization of Kynurenic Acid Occluded in Sol-Gel Silica and SBA-15 Silica as Release Reservoirs. *Journal of Nanomaterials*, *2014*(Article ID 507178), 1–9. https://doi.org/10.1155/2014/507178.

Lugo-Huitrón, R., Blanco-Ayala, T., Ugalde-Muñiz, P., Carrillo-Mora, P., Pedraza-Chaverrí, J., Silva-Adaya, D., La Cruz, V. P. (2011). On the antioxidant properties of kynurenic acid: Free radical scavenging activity and inhibition of oxidative stress. *Neurotoxicology and Teratology*, *33*(5), 538–547. https://doi.org/10.1016/j.ntt.2011.07.002.

Machín, R., Isasi, J. R., & Vélaz, I. (2012). β-Cyclodextrin hydrogels as potential drug delivery systems. *Carbohydrate Polymers*, *87*(3), 2024–2030. https://doi.org/10.1016/j.carbpol.2011.10.024.

Mognetti, B., Barberis, A., Marino, S., Berta, G., De Francia, S., Trotta, F., & Cavalli, R. (2012). In vitro enhancement of anticancer activity of paclitaxel by a Cremophor free cyclodextrin-based nanosponge formulation. *Journal of Inclusion Phenomena and Macrocyclic Chemistry*, *74*(1–4), 201–210. https://doi.org/10.1007/s10847-011-0101-9.

Moroni, F., Russi, P., Lombardi, G., Beni, M., & Carlh, V. (1988). Presence of Kynurenic Acid in the Mammalian Brain. *Journal of Neurochemistry*, *51*, 177–180. https://doi.org/10.1111/j.1471-4159.1988.tb04852.x.

Pushpalatha, R., Selvamuthukumar, S., & Kilimozhi, D. (2018). Cross-linked, cyclodextrin-based nanosponges for curcumin delivery -Physicochemical characterization, drug release, stability and cytotoxicity. *Journal of Drug Delivery Science and Technology*, *45*, 45–53. https://doi.org/10.1016/j.jddst.2018.03.004.

Schwarcz, R., Bruno, J. P., Muchowski, P. P., & Wu, H.-Q. (2013). Kynurenines in the Mammalian Brain: When Physiology Meets Pathology. *Nature Review Neuroscience*, *13*(7), 465–477. https://doi.org/10.1038/nrn3257.KYNURENINES.

Shityakov, S., Salmas, R. E., Durdagi, S., Salvador, E., Pápai, K., Yáñez-Gascón, M. J., Broscheit, J.-A. (2016). Characterization, in Vivo Evaluation, and Molecular Modeling of Different Propofol-Cyclodextrin Complexes To Assess Their Drug Delivery Potential at the Blood-Brain Barrier Level. *J. Chem. Inf. Model.*, *56*(10), 1914–1922. https://doi.org/10.1021/acs.jcim.6b00215.

Singh, A., Worku, Z. A., & Mooter, G. Van Den. (2011). Oral formulation strategies to improve solubility of poorly water-soluble drugs Oral formulation strategies to improve solubility of poorly water-soluble drugs. *Expert Opinion on Drug Delivery*, *8*(10), 1361–1378. https://doi.org/10.1517/17425247.2011.606808.

Singh, P., Ren, X., Guo, T., Wu, L., Shakya, S., He, Y., Zhang, J. (2018). Biofunctionalization of β-cyclodextrin nanosponges using cholesterol. *Carbohydrate Polymers*, *190*, 23–30. https://doi.org/10.1016/j.carbpol.2018.02.044 CARP.

Stone, T. W. (2001). Endogenous neurotoxins from tryptophan. *Toxicon*, *39*(1), 61–73. https://doi.org/10.1016/S0041-0101(00)00156-2.

Stone, T. W., & Connick, J. H. (1985). Quinolinic acid and other kynurenines in the central nervous system. *Neuroscience*, *15*(3), 597–617. https://doi.org/10.1016/0306-4522(85)90063-6.

Sundararajan, M., Thomas, P. A., Venkadeswaran, K., Jeganathan, K., & Geraldine, P. (2017). Synthesis and Characterization of Chrysin-Loaded β-Cyclodextrin-Based Nanosponges to Enhance In-Vitro Solubility, Photostability, Drug Release, Antioxidant Effects and Antitumorous Efficacy. *Journal of Nanoscience and Nanotechnology*, *17*(12), 8742–8751. https://doi.org/10.1166/jnn.2017.13911.

Swaminathan, S., Pastero, L., Serpe, L., Trotta, F., Vavia, P., Aquilano, D., Cavalli, R. (2010). Cyclodextrin-based nanosponges encapsulating camptothecin: Physicochemical characterization, stability and cytotoxicity. *European Journal of Pharmaceutics and Biopharmaceutics*, *74*(2), 193–201. https://doi.org/10.1016/j.ejpb.2009.11.003.

Torne, S., Darandale, S., Vavia, P., Trotta, F., & Cavalli, R. (2013). Cyclodextrin-based nanosponges: effective nanocarrier for tamoxifen delivery. *Pharmaceutical Development and*

Technology, *18*(3), 619–625. https://doi.org/10.3109/10837450.2011.649855.

Trotta, F., Caldera, F., Dianzani, C., Argenziano, M., Barrera, G., & Cavalli, R. (2016). Glutathione Bioresponsive Cyclodextrin Nanosponges. *ChemPlusChem*, *81*(5), 439–443. https://doi.org/10.1002/cplu.201500531.

Trotta, F., Dianzani, C., Caldera, F., Mognetti, B., & Cavalli, R. (2014). The application of nanosponges to cancer drug delivery. *Expert Opinion on Drug Delivery*, *11*(6), 931–941. https://doi.org/10.1517/17425247.2014.911729.

Trotta, F., Zanetti, M., & Cavalli, R. (2012). Cyclodextrin-based nanosponges as drug carriers. *Beilstein Journal of Organic Chemistry*, *8*, 2091–2099. https://doi.org/10.3762/bjoc.8.235.

Turski, M. P., Turska, M., Kocki, T., Turski, W. A., & Paluszkiewicz, P. (2015). Kynurenic Acid Content in Selected Culinary Herbs and Spices. *Journal of Chemistry*, *2015*, 1–6. https://doi.org/10.1155/2015/617571.

Turski, M. P., Turska, M., Zgrajka, W., Kuc, D., & Turski, W. A. (2009). Presence of kynurenic acid in food and honeybee products. *Amino Acids*, *36*(1), 75–80. https://doi.org/10.1007/s00726-008-0031-z.

Varga, N., Csapó, E., Majláth, Z., Ilisz, I., Krizbai, I. A., Wilhelm, I., Dékány, I. (2016). Targeting of the kynurenic acid across the blood-brain barrier by core-shell nanoparticles. *European Journal of Pharmaceutical Sciences*, *86*, 67–74. https://doi.org/10.1016/j.ejps.2016.02.012.

Vécsei, L., Szalárdy, L., Fülöp, F., & Toldi, J. (2013). Kynurenines in the CNS: recent advances and new questions. *Nature Reviews Drug Discovery*, *12*(1), 64–82.

https://doi.org/10.1038/nrd3793.

Venuti, V., Rossi, B., Mele, A., Melone, L., Punta, C., Majolino, D., Trotta, F. (2017). Tuning structural parameters for the optimization of drug delivery performance of cyclodextrin-based nanosponges. *Expert Opinion on Drug Delivery*, *14*(3), 331–340. https://doi.org/10.1080/17425247.2016.1215301.

Wajs, E., Caldera, F., Trotta, F., & Fragoso, A. (2013). Peroxidase-encapsulated cyclodextrin nanosponge immunoconjugates as a signal enhancement tool in optical and electrochemical assays. *Analyst*, *139*(2), 375–380. https://doi.org/10.1039/c3an01643a.

Wen, H., Jung, H., & Li, X. (2015). Drug Delivery Approaches in Addressing Clinical Pharmacology-Related Issues: Opportunities and Challenges. *The AAPS Journal*, *17*(6), 1327–1340. https://doi.org/10.1208/s12248-015-9814-9.

Woldum, H. S., Larsen, K. L., & Madsen, F. (2008). Cyclodextrin Controlled Release of Poorly Water-Soluble Drugs from Hydrogels. *Drug Delivery*, *15*(1), 69–80. https://doi.org/10.1080/10717540701829267.

Yen, G. C., Chang, Y. C., & Su, S. W. (2003). Antioxidant activity and active compounds of rice koji fermented with Aspergillus candidus. *Food Chemistry*, *83*(1), 49–54. https://doi.org/10.1016/S0308-8146(03)00035-9.

Zainuddin, R., Zaheer, Z., Sangshetti, J. N., & Momin, M. (2017). Enhancement of oral bioavailability of anti-HIV drug rilpivirine HCl through nanosponge formulation. *Drug Development and Industrial Pharmacy*, *43*(12), 2076–2084. https://doi.org/10.1080/03639045.2017.1371732.

718 Zhuravlev, A. V., Zakharov, G. A., Shchegolev, B. F., & Savvateeva-Popova, E. V. (2016).
719 Antioxidant Properties of Kynurenines: Density Functional Theory Calculations. *PLoS*
720 *Computational Biology*, *12*(11), 1–31. https://doi.org/10.1371/journal.pcbi.1005213.

721 Zidan, M. F., Ibrahim, H. M., Afouna, M. I., & Ibrahim, E. A. (2018). In vitro and in vivo
722 evaluation of cyclodextrin-based nanosponges for enhancing oral bioavailability of atorvastatin
723 calcium. *Drug Development and Industrial Pharmacy*, *44*(8), 1243–1253.
724 https://doi.org/10.1080/03639045.2018.1442844.

725